Catal Lett (2012) 142:582–587
DOI 10.1007/s10562-012-0795-3

$NiFe_2O_4@SiO_2$ Nanoparticles Stabilized by Porous Silica Shells

Nisha Shukla · Abigail Ondeck · Johanna C. Lee · James B. Miller

Received: 2 November 2011 / Accepted: 1 March 2012 / Published online: 21 March 2012

Abstract $NiFe_2O_4$ nanoparticles stabilized by porous silica shells ($NiFe_2O_4@SiO_2$) were prepared using a one-pot synthesis and characterized for their physical and chemical stability in severe environments, representative of those encountered in industrial catalytic reactors. The SiO_2 shell is porous, allowing transport of gases to and from the metal core. The shell also stabilizes $NiFe_2O_4$ at the nanoparticle surface: $NiFe_2O_4@SiO_2$ annealed at temperatures through 973 K displays evidence of surface Ni, as verified by H_2 TPD analyses. At 1,173 K, hematite forms at the surface of the metallic cores of the $NiFe_2O_4@SiO_2$ nanoparticles and surface Ni is no longer observed. Without the silica shell, however, even mild reduction (at 773 K) can draw Fe to the surface and eliminate surface Ni sites.

Keywords Nanotechnology · Nanoparticles · Nanostructure · Electron microscopy · Spectroscopy and general characterisation

1 Introduction

Ni and Fe have important applications as catalysts for Fischer–Tropsch (FT) conversion of synthesis gases to liquids and as carriers for chemical looping combustion systems. In the FT application, Ni and Fe catalysts have been used in both supported and powdered forms. Two drawbacks of powdered catalysts are low surface area and the lack of uniformity of individual particles. To overcome these challenges, the past decade has seen increased interest in synthesis of monodispersed nanoparticles for applications in catalysis. Initial efforts in synthesis of nanoparticles were aimed at control of nanoparticle size and shape [1–3]. Recently, efforts have turned towards synthesis of alloy nanoparticles [4–6]. Alloy nanoparticles can be more effective catalysts or have better magnetic properties than pure component nanoparticles [1, 7, 8]. Performance of alloy nanoparticles in applications such as FT depends on control of both composition and particle size [9–13]. However, one disadvantage of subjecting small metallic nanoparticles to the high temperatures required in catalytic reactors is that they tend to sinter or aggregate into larger particles. To prevent aggregation, there has been significant interest and success in the preparation of metal nanoparticles coated with thin shells of silica and other ceramic materials [8, 14–17]. A core–shell multi-component structure can be catalytically active if the ceramic shell is sufficiently porous to allow transport of gases to and from the surface of the metal alloy core [18]. At the same time, the shell prevents or retards sintering of the metallic alloy cores, thus allowing their use over an extended range of temperatures. The synthesis of such core–shell nanoparticles structures requires a fundamental understanding of the factors that influence their growth, structure, morphology and porosity.

In this work, we report our one-pot preparation of bimetallic FeNi alloy nanoparticles with *porous* SiO_2 shells ($NiFe_2O_4@SiO_2$). The preparation delivers nanoparticles with well-controlled shapes, sizes and compositions. We

N. Shukla · J. B. Miller
National Energy Technology Laboratory,
620 Cochrans Mill Road, Pittsburgh, PA 15236, USA

N. Shukla
Institute for Complex Engineered Systems,
Carnegie Mellon University, Pittsburgh, PA 15213, USA

A. Ondeck · J. C. Lee · J. B. Miller (✉)
Department of Chemical Engineering, Carnegie Mellon University, Pittsburgh, PA 15213, USA
e-mail: jbmiller@andrew.cmu.edu

demonstrate the porosity of the silica shell by N_2 sorption methods, and use X-ray diffraction (XRD) and temperature programmed techniques to compare the nanoparticles' stability in extreme environments to those of commercially available catalytic materials.

2 Experimental

Ni(II) nitrate hexahydrate (>99.99 %), Ni (II) chloride, Brij 56 (polyethylene glycol hexadecyl ether, average $M_n \sim 683$), Fe(II) chloride, ammonium hydroxide solution (33 % solution), propanol, tetraethyl orthosilicate (TEOS, 99 %), and cylcohexene were purchased from Sigma Aldrich and were used without purification. $NiFe_2O_4@SiO_2$ nanoparticles were synthesized using a one-pot technique. Parameters used for synthesis of spherical and rod-shaped $NiFe_2O_4@SiO_2$ are summarized in Table 1. In a typical preparation, Brij 56 surfactant was dissolved in 100 mL of cyclohexene and stirred in a three-neck glass flask for 30 min at ~342 K, forming a clear solution. Next, 4 mL of an aqueous solution of Fe(II) chloride solution was added; the mixture turned yellow. After stirring for 10 min, 4 mL of an aqueous solution of Ni(II) nitrate hexahydrate was added to the reaction mixture. Next, 30 % aqueous NH_4OH solution was added; the solution turned blue, then grey, then black. The reaction mixture was heated for another 10 min before drop-wise addition of a solution of TEOS in methanol. The final reaction mixture was heated and stirred for another 15 min–1 h. Product $NiFe_2O_4@SiO_2$ nanoparticles were centrifuged and washed with polar solvent to remove excess surfactant.

Relative solution amounts and concentrations were varied, as shown in Table 1, to change the geometry of the product nanoparticles. The main factor that determines nanoparticle shape is the concentration of surfactant (Brij 56). The surfactant concentration used to prepare nanorods is twice that used for nanospheres [19]. Except for the TEM images, all characterizations reported in this work are for nanosphere samples.

Table 1 Parameters for preparation of $NiFe_2O_4@SiO_2$

Parameter	Nanospheres	Nanorods
Brij concentration (M in cyclohexane)	0.125	0.25
Fe(II) chloride concentration (M)	0.8	0.6
Ni(II) nitrate hexahydrate concentration (M)	0.5	0.6
Volume of 30 % aqueous NH_4OH solution (mL)	16.5	6.0
Volume of TEOS in methanol solution (mL)	23	50

2.1 X-ray Diffraction (XRD) and X-ray Fluorescence (XRF)

XRD patterns were acquired on a Panalytical X'Pert Pro X-ray diffractometer. A Cu radiation source was used with a polycapillary lens and a Ni filter on the incident beam. Nanoparticle samples were prepared for XRD by drying overnight at 373 K in a vacuum oven, followed by annealing in air at temperatures from 773 to 1,173 K in a box-furnace. XRF measurements were performed on a Panalytical MiniPal 4 XRF spectrometer. Annealed samples were placed in a plastic cup with a bottom X-ray window made of polyvinylidene chloride (Saran Wrap). A rhodium target X-ray source was used with 15 kV and 0.28 mA power settings. Scans were run for 30 s in air with no filter.

2.2 Transmission Electron Microscopy (TEM)

TEM studies were conducted using a JEOL JEM-2000 EX II microscope operating at 200 keV with a Gatan Camera. The high-resolution TEM studies were performed using a Technai F20 FEG/HRTEM/STEM with a Gatan imaging filter and an energy dispersive X-ray spectroscopy system. TEM samples were prepared by evaporation of 20 μL of the colloidal $NiFe_2O_4@SiO_2$ nanoparticle solution in propanol onto a carbon-coated, 200 mesh, Cu TEM grid.

2.3 Characterization of Shell Porosity by N_2 Sorption

The pore size distribution and surface area of the nanoparticles were measured by N_2 sorption methods using a Quantachrome Nova 2200e instrument. Surface areas were calculated using the BET method; pore size distributions were determined from desorption isotherms. Nanoparticle samples were prepared for characterization by drying overnight at 373 K in a vacuum oven, followed by annealing in air at 773 K for 1 h in a box furnace.

2.4 Temperature Programmed Reduction (TPR) and Temperature Programmed Desorption (TPD) Measurements

TPR and H_2-TPD experiments were performed using a Micromeritics AutoChem HP 2950 instrument. Before characterization, samples of $NiFe_2O_4@SiO_2$ nanoparticles and an uncoated reference were annealed in air for 1 h in a box furnace at temperatures between 773 and 1,173 K. Approximately 0.065 g of $NiFe_2O_4@SiO_2$, or 0.013 g of uncoated $NiFe_2O_4$ sample, was loaded into the instrument's stainless steel reactor. Once in the reactor, the sample was dried at 623 K in flowing He for 30 min. Then, after cooling to 323 K, the gas flow was changed to 10 % H_2 in

Ar and the sample was heated to 773 K at 10 K/min. The sample was held at 773 K for 60 min. During both heating and the hold at 773 K, hydrogen consumption by the sample was measured by comparing the thermal conductivities of the gas streams on the inlet and outlet sides of the reactor. The sample was then cooled to 193 K while still under H_2/Ar flow. After 30 min at 193 K in H_2/Ar, the flow was changed to pure Ar. After 30 min in Ar at 193 K, the sample was heated at 10 K/min to 773 K. The sample was held at 773 K for 30 min. Desorption of hydrogen from the sample during both heating and the hold at 773 K was monitored by mass spectrometry (signal at m/e = 2). A NiO/SiO_2–Al_2O_3 catalyst (66 wt% Ni) and Fe_2O_3 powder (5 μ, 99 %) were obtained from Alfa-Aesar for use as single metal references for the TPR and TPD experiments.

3 Results and Discussion

The size and morphology of the $NiFe_2O_4$@SiO_2 nanoparticles were examined using TEM. Figure 1 shows typical examples of bright field TEM images of $NiFe_2O_4$@SiO_2 nanoparticles synthesized using the one-pot synthesis. By adjusting preparation parameters, either spherical (Fig. 1a) or rod-shaped (Fig. 1b) $NiFe_2O_4$@SiO_2 nanoparticles can be prepared. Within the silica shell, the $NiFe_2O_4$ nanoparticle cores are either irregular or rod-shaped.

$NiFe_2O_4$@SiO_2 nanosphere samples were annealed in air before structural characterization by XRD. Figure 2a shows the XRD pattern of $NiFe_2O_4$@SiO_2 nanoparticles annealed at 773 K for 1 h. Diffraction peaks are observed at 2θ = 30.29, 35.69, 37.31, 43.36, 53.80, 57.35, 62.91 and 74.6°. This pattern is characteristic of $NiFe_2O_4$, suggesting formation of nickel ferrite nanoparticles with inverse spinel structure [20, 21]. The sharpness of the diffraction features indicates that the sample is highly crystalline. The atomic ratio of Fe:Ni in the sample, measured by XRF, is 1.3:1; this ratio is consistent with the ratio of the precursors used in preparation of the sample. Fe:Ni for the spinel is expected to be 2:1, thus it is possible that this sample contains X-ray amorphous Ni oxides. Figure 2b shows the diffraction pattern of the same sample after annealing at 1,173 K. New features appear at 24.00, 33.15, 40.85, and 65.47°, indicating the formation of an independent hematite (Fe_2O_3) phase that coexists with the spinel [22, 23].

The diffraction patterns of silica coated $NiFe_2O_4$ nanoparticles were compared to those of spherical $NiFe_2O_4$ nanoparticles *without* silica coating. Figure 3 shows the XRD pattern of $NiFe_2O_4$ nanoparticles without silica coatings annealed at 973 K in air for 1 h. The pattern is

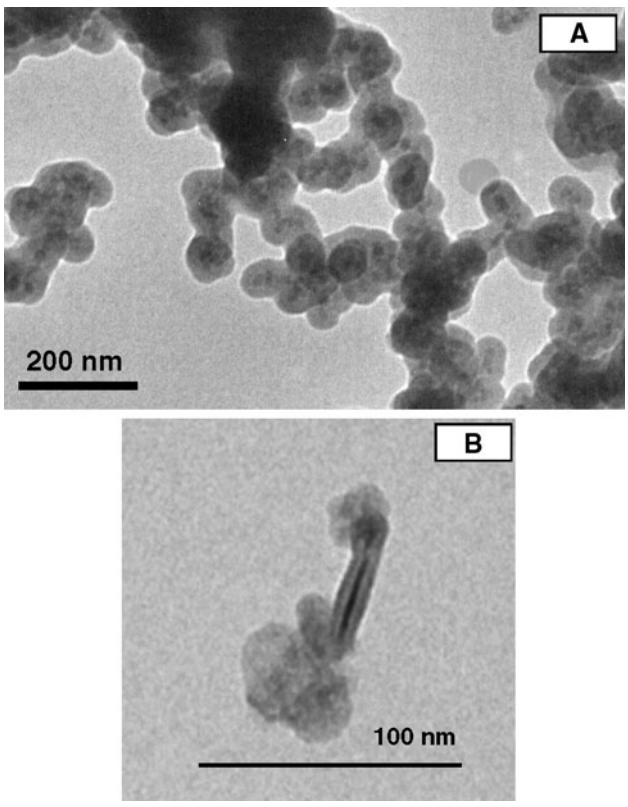

Fig. 1 Bright field TEM images of $NiFe_2O_4$@SiO_2 nanoparticles packed to form nanospheres (**a**) or nanorods (**b**). The silica shell is 10–20 nm thick

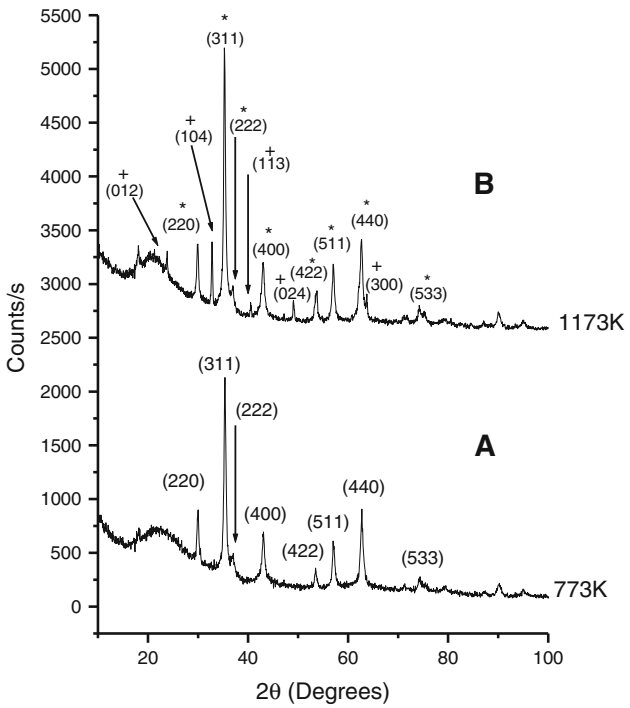

Fig. 2 XRD patterns of $NiFe_2O_4$@SiO_2 nanoparticles annealed at 773 K (**a**) and 1,173 K (**b**). *Asterisk* indicates diffraction features of $NiFe_2O_4$. *Plus* indicates diffraction features of hematite (Fe_2O_3)

characteristic of nickel ferrite, with no evidence of hematite. The ratio of Fe:Ni in the uncoated sample, as measured by XRF, is 0.8:1. As was the case for the SiO_2 coated nanoparticles, this ratio suggests Ni content in excess of that expected for a stoichiometric spinel; X-ray amorphous Ni oxides may also be present in this sample. Interestingly, the relative intensities of the uncoated $NiFe_2O_4$ diffraction features differ from those of the $NiFe_2O_4$@SiO_2 (Fig. 2). For example, the (400) reflection dominates the pattern of uncoated $NiFe_2O_4$, but it is a minor feature in the pattern of the SiO_2-coated material. This difference suggests that preparation parameters—including the presence of the coating—can be leveraged to direct the direction of nanoparticle crystal growth.

To be useful for catalysis, the $NiFe_2O_4$ cores must be accessible by reactant molecules, thus the silica coating must be porous. The porosity of the silica coating was characterized by N_2 sorption methods. Figure 4 shows the pore size distribution of $NiFe_2O_4$@SiO_2 nanoparticles annealed at 773 K. The pore size distribution displays a sharp maximum at ~3.7 nm; this is the characteristic diameter of the pores in the silica shells [24]. The surface area of this sample, determined by BET analysis, is 72 m^2/g. These results are comparable to those we previously reported for SiO_2 coatings on Ni nanorods [25].

Figure 5 compares the TPR spectra of uncoated $NiFe_2O_4$ nanospheres annealed in air at 773 K and $NiFe_2O_4$@SiO_2 nanospheres annealed at 773, 973, and 1,173 K. TPR spectra for commercially available NiO/SiO_2–Al_2O_3 and Fe_2O_3, both annealed at 773 K, are included as references. The $NiFe_2O_4$ samples generally display two features; in the uncoated sample, the first feature appears at 648 K and the second as a shoulder between ~680 and 770 K. TPR features in the range 600–700 K have been associated with reduction of NiO to Ni and Fe_2O_3 to Fe_3O_4 [26–31]. The single component Fe_2O_3 sample shows a small feature at 640 K, likely due to reduction of Fe_2O_3–Fe_3O_4; a large feature at higher temperature indicates further reduction of Fe [30, 31]. The NiO-only sample presents a pair of peaks, which are generally explained by reduction of NiO that is stabilized to different extents by its support [26, 32].

The reduction profile of the uncoated $NiFe_2O_4$ sample more closely resembles that of the NiO reference than that of the Fe_2O_3 reference. The predominant low-temperature feature of uncoated $NiFe_2O_4$ likely corresponds to reduction to Ni + Fe_2O_3. As shown in Fig. 6, the XRD pattern of this sample after TPR/D confirms formation of Fe_2O_3. The appearance of this reduction feature at a higher temperature than in the Ni reference suggests that $NiFe_2O_4$ is

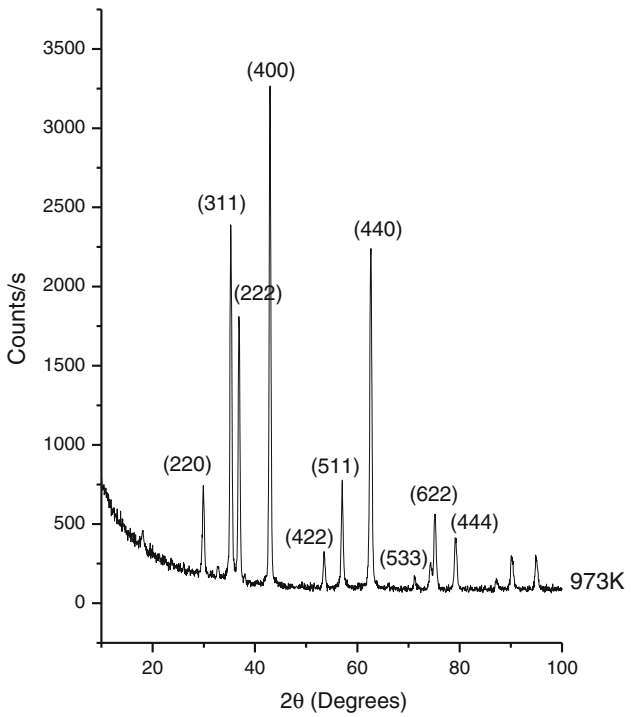

Fig. 3 XRD pattern of $NiFe_2O_4$ nanoparticles without silica coating annealed at 973 K

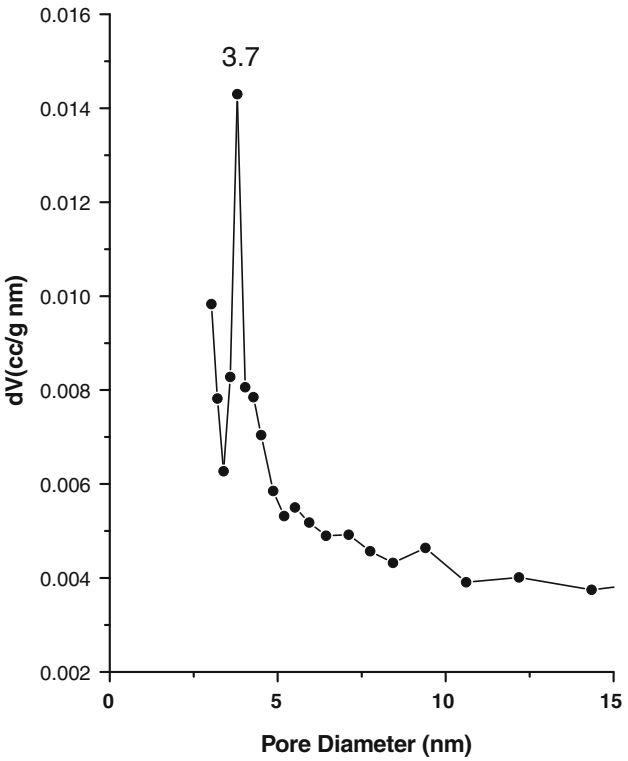

Fig. 4 Pore size distribution, measured by N_2 desorption, of $NiFe_2O_4$@SiO_2 nanoparticles annealed at 773 K

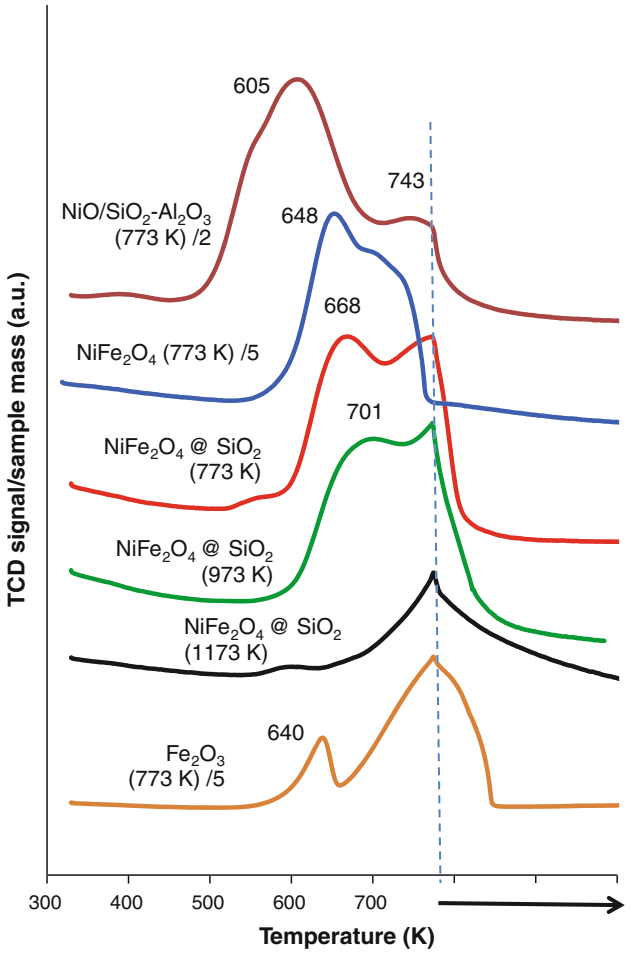

Fig. 5 Temperature programmed reduction of $NiFe_2O_4$@SiO_2 (annealed at different temperatures) and $NiFe_2O_4$ nanoparticles; and NiO and Fe_2O_3 reference samples

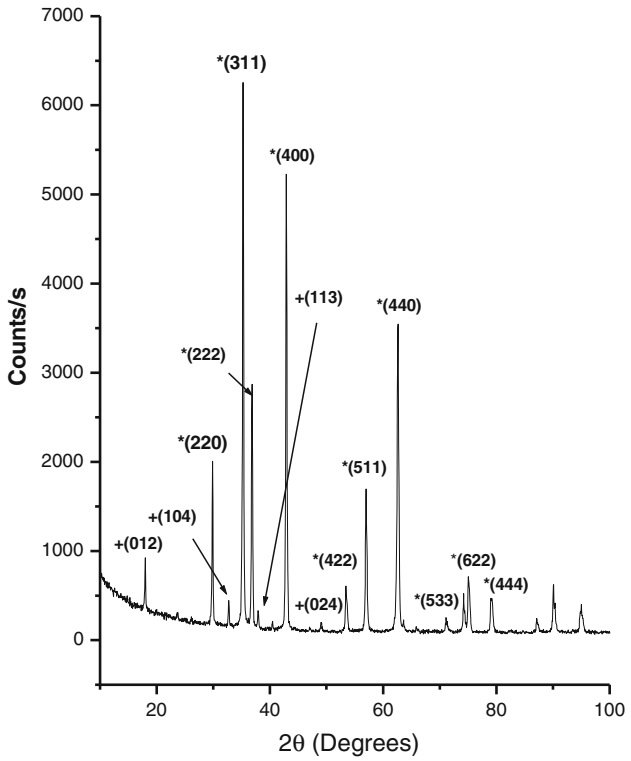

Fig. 6 Post TPR/D XRD pattern of $NiFe_2O_4$ nanoparticles without silica. *Asterisk* indicates diffraction features of $NiFe_2O_4$. *Plus* indicates diffraction features of hematite (Fe_2O_3)

more stable than NiO. Coating the $NiFe_2O_4$ with silica further stabilizes the oxide and delays its reduction to higher temperatures. As $NiFe_2O_4$@SiO_2 is annealed at higher temperatures, both reduction features move to higher temperatures. When annealed at 1,173 K, relatively little reduction of $NiFe_2O_4$@SiO_2 is observed; its reduction profile now resembles that of the Fe_2O_3 reference. This result is consistent with the XRD pattern of SiO_2@$NiFe_2O_4$ annealed at 1,173 K, which displayed features of both $NiFe_2O_4$ and Fe_2O_3 (Fig. 3). Fe_2O_3 formed by aggressive oxidation of $NiFe_2O_4$@SiO_2 may segregate to the surface of the nanoparticle and delay reduction of underlying Ni-containing species.

H_2-TPD spectra for the same six samples are compared in Fig. 7. The Fe_2O_3 reference sample adsorbs little hydrogen in this experiment. The NiO reference, on the other hand, shows three features, which have been ascribed to H in three different surface regions of Ni: sub-surface (α), "second-layer" (β), and top-surface (γ) [33]. $NiFe_2O_4$@SiO_2 annealed at 773 and 973 K display the α and γ desorption features; β appears as a separate feature in the 973 K sample. Clearly, H_2 adsorbs onto Ni sites in these samples. However, when $NiFe_2O_4$@SiO_2 is annealed at 1,173 K, only a small α feature remains; the γ peak, characteristic of top-surface Ni, is no longer present. The uncoated $NiFe_2O_4$ displays none of the features characteristic of desorption of hydrogen from Ni; instead, it bears a strong resemblance to the TPD spectrum of the Fe_2O_3 reference.

Our results suggest that the SiO_2 shell stabilizes Ni at the nanoparticle surface; after reduction at 773 K, $NiFe_2O_4$@SiO_2 annealed at temperatures through 973 K show clear evidence of surface Ni in their H_2-TPD spectra. Oxidation at 1,173 K induces conversion to Fe_2O_3, which, as noted earlier, may segregate to the nanoparticle surface and obscure Ni atoms. Without the shell, reduction at 773 K can draw Fe to the surface, and eliminate surface Ni sites.

4 Conclusion

We demonstrate a one-pot synthesis for $NiFe_2O_4$@SiO_2 nanoparticles. Nitrogen desorption experiments show that the silica coatings are porous, with pore diameter $\sim$3.7 nm.

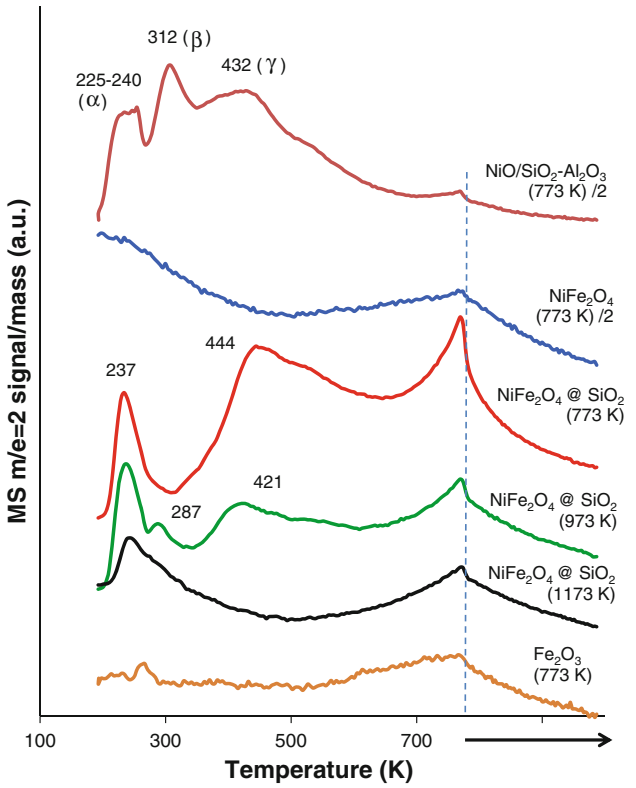

Fig. 7 H_2 temperature programmed desorption spectra of $NiFe_2O_4$@SiO_2 (annealed at different temperatures) and $NiFe_2O_4$ nanoparticles; and NiO and Fe_2O_3 reference samples. Samples were exposed to H_2 at 193 K

The coating stabilizes the $NiFe_2O_4$ cores against reduction to hematite (Fe_2O_3) and preserves surface Ni sites.

Acknowledgment This effort was performed in support of the National Energy Technology Laboratory's on-going research in "Next generation, sinter-resistant, catalysts for syngas conversion", under the RES contract DE-FE0004000. JBM thanks Sittichai Natesakhawat (NETL-Pittsburgh) for advice on the TPR/D experiments.

References

1. Rioux RM, Song H, Grass M, Habas S, Niesz K, Hoefelmeyer JD, Yang P, Somorjai GA (2006) Top Catal 39(3–4):167
2. Shukla N, Svedberg EB, Ell J (2006) Surf Coat Tech 201(6):3810
3. Wang ZL, Petroski JM, Green TC, El-Sayed MA (1998) J Phys Chem B 102(32):6145
4. Tang W, Zhang L, Henkelman G (2011) J Phys Chem Lett 2:1328
5. Park KW, Han DS, Sung YE (2006) J Power Sources 163:82
6. Maye MM, Luo J, Han Li, Kariuki N, Rab Z, Khan N, Naslund HR, Zhong CJ (2004) Prepr Pap Am Chem Soc Div Fuel Chem 49(2):938
7. Jeyadevan B, Shinoda K, Justin RJ, Matsumot T, Sato K, Takahashi H, Sato Y, Tohji K (2006) IEEE Trans Magn 42(10): 3030
8. Takenaka S, Umebayashi H, Tanabe E, Matsune H, Kishida M (2007) J Catal 245(2):392
9. Ishihara T, Eguchi K, Arai H (1987) Appl Catal 30:225
10. Arcuri KB, Schwartz LH, Piotrowski RD, Butt JB (1984) J Catal 85:349
11. de la Peña O'Shea VA, Álvarez-Galván MC, Campos-Martín JM, Fierro JLG (2007) Appl Catal A 326:65
12. Kuila D, Nagineni VS, Zhao S, Indukuri H, Liang Y, Potluri A, Siriwardane U, Seetala N, Fang J (2004) Mat Res Soc Symp Proc 820:03.4.1
13. Lo JMH, Ziegler T (2008) J Phys Chem C 112:13642
14. Liu C, Wu XW, Klemmer T, Shukla N, Weller D (2005) Chem Mater 17(3):620
15. Liz-Marzan LM, Giersig M, Mulvaney P (1996) Langmuir 12(18):4329
16. Lu Y, Yin YD, Li ZY, Xia YA (2002) Nano Lett 2(7):785
17. Tago T, Shibata Y, Hatsuta T, Miyajima K, Kishida M, Tashiro S, Wakabayashi K (2002) J Mater Sci 37(5):977
18. Joo SH, Park JY, Tsung CK, Yamada Y, Yang PD, Somorjai GA (2009) Nat Mater 8(2):126
19. Shukla N, Nigra MM, Bartel MA, Nigra AM, Gellman AJ (2011) J Nanosci Nanotech 11:2480
20. Deb P, Basumallick A, Das A (2007) Solid State Comm 142:702
21. Carta D, Loche D, Mountjoy G, Navarra G, Corrias A (2008) J Phys Chem C 112:15623
22. Jing Z, Wu S (2004) Mater Lett 58:3637
23. Sepelak V, Bergmann I, Feldhoff A, Heitjans P, Krumeich F, Menzel D, Litterst FJ, Campbell SJ, Becker KD (2007) J Phys Chem 111:5026
24. Yao X, Zhang L, Wang S (1995) Sens Actuators B 24–25347:347
25. Shukla N, Miller J, Coletta E, Ondeck A, Pushkarev V, Gellman A (2011) Catal Lett 141:491
26. Ermkova MA, Ermakov DY (2002) Catal Today 77:225
27. Borowieki T, Denis A, Gac W, Dziembaj R, Piwowarska Z, Drozdek M (2004) Appl Catal A 274:259
28. Li J, Lu G (2004) Appl Catal A 273:163
29. Venugopal A, Kumar SN, Ashok J, Prasad DH, Kumari VD, Prasad KBS, Subrahmanyan M (2007) Int J Hydrog Energy 32:1782
30. Yu Z, Chen D, Ronning M, Vralstad T, Ochoa-Fernandez E, Holmen A (2008) Appl Catal A 338:136
31. Batista AHD, Ramos FSO, Braga TP, Lima CL, deSousa FF, Barros EBD, Filho JM, deOliveira AS, deSousa JR, Valentini A, Oliveria AC (2010) Appl Catal A 382:148
32. He S, Jing Q, Yu Y, Mo L, Lou H, Zheng X (2009) Catal Today 148:130
33. Znak L, Zielinski J (2008) Appl Catal A 334:268